Reduction of Dioxygen by a Dimanganese Unit Bonded Inside a Cavity Provided by a Pyrrole-Based Dinucleating Ligand

Federico Franceschi,[a] Geoffroy Guillemot,[a] Euro Solari,[a] Carlo Floriani,*[a] Nazzareno Re,[b] Henrik Birkedal,[c] and Philip Pattison[c]

Abstract: A novel class of dinucleating ligands has been introduced into manganese chemistry to study the reactivity of this metal towards dioxygen under strictly controlled conditions. Such N_4 ligands combine some of the major peculiarities of tetradentate Schiff bases and the porphyrin skeleton. They are derived from the condensation between 2-pyrrolaldehyde and ethylenediamine or *o*-phenylenediamine, leading to pyrenH$_2$ (LH$_2$, **1**), pyrophenH$_2$ (L′H$_2$, **2**) and Me$_2$pyrophenH$_2$, (L″H$_2$, **3**), respectively. Their metallation with [Mn$_3$(Mes)$_6$] (Mes = 2,4,6-trimethylphenyl) led to [Mn$_2$L$_2$] (**4**), [MnL′(thf)$_2$] (**5**) and [MnL″(thf)$_2$] (**6**). Complex **4** displays a double-stranded helical structure, while **5** and **6** are mononuclear complexes containing hexacoordinated metals. Regardless of their structure, complexes **5** and **6** behave in a similar manner to **4** in their reaction with dioxygen, namely, as a dimetallic unit inside a cavity defined by two dinucleating ligands. These reactions led to dinuclear Mn^{III}/Mn^{IV} oxo-hydroxo derivatives, [Mn$_2$L$_2$(μ-O)(μ-OH)] (**7**), [Mn$_2$L′$_2$(μ-O)(μ-OH)] (**8**) and [Mn$_2$L″$_2$(μ-O)(μ-OH)] (**9**), in which the two Mn ions are strongly antiferromagnetically coupled [$J = -53$ (**7**), $J = -64$ (**8**), $J = -60$ cm^{-1} (**9**)]. The crystal structure of **7** could only be solved with synchrotron radiation as the crystals diffracted very poorly and suffered from twisting and disorder. The formation of **7**–**9** has been proposed to occur through the formation of an intermediate dinuclear hydroperoxo species.

Keywords: N ligands · manganese · oxygen reduction · Schiff bases · structural elucidation

Introduction

The redox chemistry of Mn^{II} in a macrocyclic environment has so far attracted a lot of attention within the context of modeling studies on photosystem II,[1] and of the Mn-assisted catalytic oxygen transfer. Within this context, the reaction of Mn^{II} with dioxygen is by far the most intriguing, but the least often used for producing active Mn-oxo derivatives. Some of the facets of this reaction have been explored during this study, taking advantage of several novel approaches and starting materials. Two general classes of compounds have been widely used to date: the porphyrin derivatives[2] and, more recently, the tetradentate Schiff base derivatives[3] exemplified by [Mn(tpp)] (tpp = tetraphenylporphyrin dianion) and [Mn(salen)] (salen = *N*,*N*′-ethylene-bis(salicylideneiminato) dianion). The two ligands, which differ very much in the nature of their donor atoms, aromaticity and constituting organic groups, have different advantages that would be useful to combine in a single molecule. With this in mind, for our studies of Mn chemistry, we recently moved to the synthesis and the use of a novel class of tetradentate ligands that are reminiscent of these two kinds of ligands. Let us consider, at this preliminary stage, some peculiarities of the ligands investigated in this work (Scheme 1) in relation to the ligands in [Mn(tpp)] and [Mn(salen)]: i) the presence of pyrrolyl anions and a set of four nitrogen donor atoms, as in

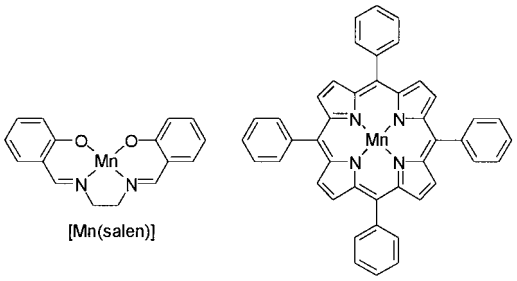

[a] Prof. Dr. C. Floriani, Dr. F. Franceschi, G. Guillemot, Dr. E. Solari
Institut de Chimie Minérale et Analytique
Université de Lausanne, BCH, 1015 Lausanne (Switzerland)
Fax: (+41) 21-6923905
E-mail: carlo.floriani@icma.unil.ch

[b] Prof. Dr. N. Re
Facoltà di Farmacia, Università degli Studi "G. D'Annunzio"
66100 Chieti (Italy)

[c] H. Birkedal, Dr. P. Pattison
Institut de Cristallographie
Université de Lausanne, BSP, 1015 Lausanne (Switzerland)

0947-6539/01/0707-1468 $ 17.50+.50/0

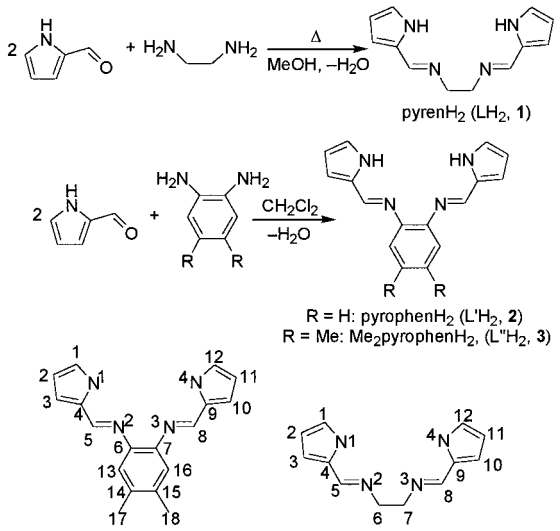

Scheme 1. The synthesis of the N_4 tetradendate Schiff bases and the labelling scheme of the ligands.

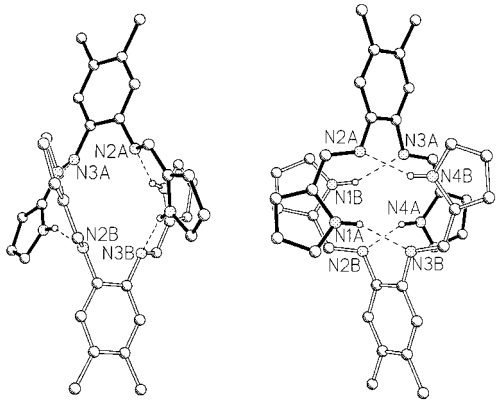

Figure 1. XP view of complex **3** showing the two independent hydrogen-bonded molecules of the asymmetric unit. Left: the view emphasising the helical, cavity forming, hydrogen-bonded complex. Right: view (rotated by 90° with respect to the view on the left) to show the individual hydrogen bonds.

the porphyrin skeleton; ii) the "open-macrocycle" structure as in the case of salicylaldehyde-derived Schiff bases;[4] iii) a very different degree of aromaticity and geometric flexibility between **1**, **2**, and **3**; the last two have a greater degree of aromaticity and impose a square-planar coordination on the metal.

The compounds derived from the metallation of LH_2 (**1**), $L'H_2$ (**2**) and $L''H_2$ (**3**) allowed us to face some of the key problems in the reduction of dioxygen by Mn^{II} macrocycles: i) the reaction of dioxygen under strictly controlled and aprotic conditions, with the well-defined and structurally characterised Mn^{II} complexes mentioned above; ii) the relevance or not of the use of preorganised dinuclear complexes; iii) the dehydrogenating ability of the superoxo or oxo intermediates.

The magnetic properties of the μ-oxo-μ-hydroxo mixed valence Mn^{III}/Mn^{IV} complexes have been fully characterised and a theoretical study has been carried out to quantify the difference in the frontier orbitals between the model compounds [Mn(tpp)] and [Mn(salen)], and the Mn^{II} compounds of this report.

Results and Discussion

Synthesis of the Mn^{II} complexes: The synthesis of LH_2 (**1**) and $L'H_2$ (**2**) has been improved up to the multigram scale; the use of a symmetric disubstituted phenylenediamine allowed us to prepare $L''H_2$ (**3**), a more lipophilic version of the $L'H_2$ ligand. All the ligands were fully characterised, including an X-ray analysis of **3** (Figure 1). In the crystal structure of **3** there are two molecules in the asymmetric unit. In addition to these, one strongly disordered CCl_4 solvent molecule is present. The two molecules are bound together in a helical dimer by N–H···N hydrogen bonds (Figure 1). The N4–H4···N2 hydrogen bonds are stronger (as determined by the donor–acceptor distances, D···A) than the N1–H1···N3 hydrogen bonds.[5] The difference in the D···A distances is 0.043(3) and 0.071(3) Å for the A and B molecule, respectively. The difference between the two independent molecules is a consequence of a shorter N4–H4···N2 hydrogen bond in B than in A, combined with a longer N1–H1···N3 hydrogen bond. The dimer is asymmetric and the *o*-phenylene rings are not perpendicular, but have an angle of 79.85(6)° between them. Furthermore, the molecules are not equally distributed about the *o*-phenylene ring planes: C6A and C6B almost lie in these planes; the distances from their respective planes being 0.087(5) Å for C6A and 0.190(4) Å for C6B. The corresponding distances for C7A and C7B are 1.468(5) Å and −1.184(4) Å, respectively. Thus, while C6A and C7A are on the same side of the BB plane, C6B and C7B are on opposite sides. It is not clear to what degree these asymmetries are the result of differences in hydrogen bonding or of close packing requirements which induce asymmetric hydrogen bonding.

The metallation of ligands **1**–**3** has been pursued by means of a conventional organometallic methodology. The reaction of the very reactive $[Mn_3(Mes)_6]\cdot$toluene (Mes = 2,4,6-trimethylphenyl) with protic ligands leads to the elimination of mesitylene and the metallation of the ligand without the formation of an additional salt, which would have had to be separated from the expected product of the reaction. The reactions were carried out in toluene or THF and gave **4**–**6** in almost quantitative yields as microcrystalline solids (Scheme 2). Compounds **4** and **5** were also characterised by X-ray analysis. The structure of **4** was particularly surprising. Unlike the analogous salen derivatives, L acts as a binucleating ligand and leads to the formation of a saturated double-stranded homotopic helicate[6] $[Mn_2L_2]$, as proven by the X-ray structural analysis (Figure 2). Crystals of **4** were grown either in toluene or THF and, surprisingly in the latter case, we did not observe coordination of a THF molecule as a fifth ligand on the manganese atoms, which remained tetracoordinate. The Mn···Mn distance is almost 4 Å (Table 1). The twist of the ligands around the Mn···Mn vector creates a cavity (Figure 2), although it is far too small for any atoms to enter without deformation of the framework. Manganese lies out of the mean ligand planes. It is 0.171(10) Å above the N1A-C1A-C2A-C3A-C4A-C5A-C6A plane and 0.148(11) Å below the

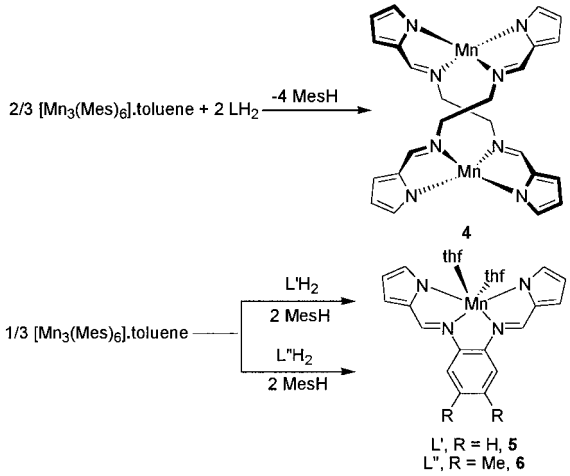

Scheme 2. The synthesis of the manganese(II) complexes.

corresponding B plane. The A plane is parallel to the symmetry-generated B plane (generated by applying $-x$, y, $-z-0.5$), with the mean distance of a B plane atom to the A plane being 3.23 Å. The overall geometry of **4** is somewhat similar to that of **3**. This is an example of the complementary use of hydrogen bonding and metal complexation to obtain a specific arrangement of ligands.

To date, the only structurally characterised compound containing L available in the Cambridge structural database (CSD)[7] was the Cu^{II} $[Cu_2L_2]$ complex,[8] which has the same connectivity as **4**. The coordination geometry of the two metal ions is, however, significantly different: the Cu^{II} centre has a

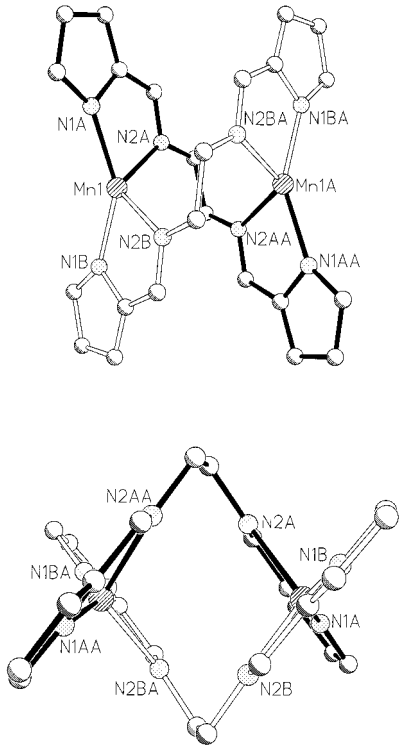

Figure 2. XP view of complex **4**. Two orientations are shown, top: emphasising the helical structure of the complex and bottom: the cavity.

quasi square-planar geometry, while coordination around the Mn^{II} centre is almost tetrahedral. This is reflected in the details of the coordination geometry. The angles between the

Table 1. Selected bond lengths [Å] and angles [°] for **4**, **5**, **7**, and **9**.

Compound 4					
Mn1–N1A	2.072(6)	Mn1–N2A	2.185(6)	Mn1–Mn1A[a]	3.997(6)
Mn1–N1B	2.085(6)	Mn1–N2B	2.170(7)		
N1A–Mn1–N2A	79.3(2)	N1A-Mn1-N1B	150.6(3)	N1A-Mn1-N2B	117.9(3)
N2A-Mn1-N1B	113.0(2)	N2A-Mn1-N2B	120.2(2)	N1B-Mn1-N2B	80.1(3)
N2A-C6A-C6AA[a]-N2AA[a]	– 64.0(1.3)	C5A-N2A-C6A-C6AA[a]	170.8(8)	N2B-C6B-C6BA[a]-N2BA[a]	63.8(1.2)
C5B-N2B-C6B-C6B[i]	173.2(8)				
Compound 5					
	complex A	complex B		complex A	complex B
Mn1–N1	2.191(9)	2.204(9)	Mn1–O1B	2.253(7)	2.225(8)
Mn1–N4	2.203(9)	2.177(9)	Mn1–O1A	2.272(8)	2.258(8)
Mn1–N2	2.249(8)	2.227(9)	Mn1–N3	2.250(9)	2.233(9)
Compound 7					
Mn1–Mn1A[b]	2.6943(12)	Mn1–O1	1.812(3)	Mn1–O1A[b]	1.812(3)
Mn1–N1A	2.058(9)	Mn1–N2A	1.982(8)	Mn1–N3B	1.956(7)
Mn1–N4B	2.068(9)	Mn1A[b]–N1B	1.949(9)	Mn1A[b]–N2B	2.043(8)
Mn1A[b]–N3A	2.074(7)	Mn1A[b]–N4A	1.960(9)		
O1-Mn1-O1A[b]	83.96(11)	Mn1-O1-Mn1A[b]	96.04(11)		
N2A-C6A-C7A-N3A	45.0(1.4)	N2B-C6B-C7B-N3B	41.4(1.4)	C5A-N2A-C6A-C7A	89.4(1.0)
C5B-N2B-C6B-C7B	94.3(1.0)	C8A-N3A-C7A-C6A	91.8(1.0)	C8B-N3B-C7B-C6B	92.6(1.0)
Compound 9					
Mn1–N1A[c]	2.041(7)	Mn1–N2A[c]	2.063(6)	Mn1–N3	2.057(6)
Mn1–N4	2.029(7)	Mn1–O1	1.853(5)	Mn1–O1A[c]	1.825(5)
Mn1–Mn1A[c]	2.659(3)	O1–O1A[c]	2.543(10)		
O1A[c]-Mn1-O1	87.4(2)	Mn1-O1-Mn1A[c]	92.6(2)	C4-C5-N2-C6	– 177.8(7)
C9-C8-N3-C7	– 178.1(6)	C5-N2-C6-C7	– 132.5(8)	C8-N3-C7-C6	127.6(8)
N2-C6-C7-N3	2.2(1.2)				

[a] Atom generated through symmetry operation $-x$, y, $-y-0.5$. [b] Atom generated through symmetry operation $-x$, $1-y$, $2-z$. [c] Atom generated through symmetry operation $1-x$, $-y$, $-z$.

0947-6539/01/0707-1470 $ 17.50+.50/0 *Chem. Eur. J.* **2001**, *7*, No. 7

N1-C1-C2-C3-C4-C5-C6 planes in the two structures are 76.1(2)° in **4**, but only 35.0° in $[Cu_2L_2]$. The N-Mn-N angles in **4** are 80.1(3)° (N1B-Mn1-N2B), 79.3(2)° (N1A-Mn1-N2A), 150.6(3)° (N1A-Mn1-N1B), 117.9(3)° (N1A-Mn1-N2B), 113.0(2)° (N1B-Mn1-N2A) and 120.2(2)° (N2B-Mn1-N2A), while in $[Cu_2L_2]$ the corresponding angles are 84.0° (N1A-Cu-N2A), 158.9° (N1A-Cu-N1B) and 100.0° (N1A-Cu-N2B). Thus, while neither case is clear-cut, it is evident that **4** is closer to a tetrahedral coordination and $[Cu_2L_2]$ is closer to square-planar. The geometric flexibility derived from the ethylene bridge can allow the ligand to satisfy the steric demand of the transition metal: in the case of Mn^{II} and Cu^{II}, a distorted coordination is mainly preferred by the metals, which forces the *trans* arrangement of the two halves of the tetradentate ligand and thus forms a dimeric unit, like **4**. In contrast, Ni^{II} clearly prefers a square-planar salen-type coordination in the [NiL] complex,[9] while Ru^{II} shows another different, transoid ligand arrangement in the monomeric [(cod)RuL] complex[10] (cod = 1,5-cyclooctadiene). A dimeric structure for the $[Zn_2L_2]$ complex has been proposed on the basis of mass spectroscopy.[11]

We analysed the conformational stability of LH_2 and $L'H_2$ by PM3 calculations with Gaussian 98.[12] A relaxed potential-energy scan was made for the N2-C6-C7-N3 torsion angle. The corresponding conformational energy line is shown in Figure 3. Note that the potential energy is very different for the

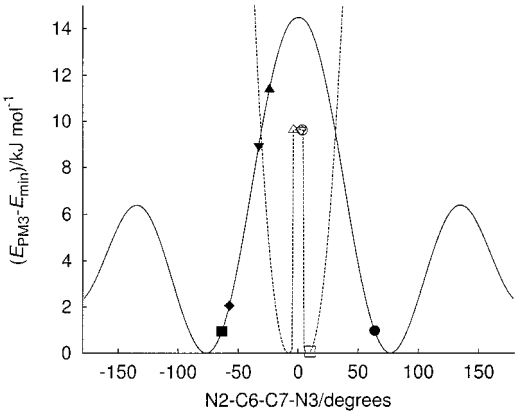

Figure 3. Conformational energy versus N2-C6-C7-N3 torsion angle in LH_2 (——) and $L'H_2$ (- - - -). **4**A ■, **4**B ●, [NiL] ▲, [RuL(cod)] ▼, $[Cu_2L_2]$ ◆, **3**A □, **3**B ○, **5**A △, **5**B ▽, **9** ◇.

two ligands. LH_2 is very flexible with minima in the potential energy $\approx \pm 77°$. All energies are small, the central barrier is only 14.5 kJ mol^{-1} (note that this energy difference can only be considered to be qualitatively correct because of the low level of the present calculations). In the case of $L'H_2$, the situation is different. The minimum energy is, as expected, $\approx 0°$. The local maximum at 0° is caused by repulsions between the hydrogens and the true minima are at ±8°. The shape of the curve confirms the intuitive image of the two ligands stated in the introduction. Ligand L is very flexible while L′ is rigid with a strong propensity to be close to planar. As can be expected, all of the structures which contain L′ are all close to the potential energy minimum. Note that the zero-centered local maximum is not necessarily present in anionic systems. For L, the situation is somewhat different. In **4** and the similar copper complex, the geometry is close to the minima found in the isolated ligand calculation. In the [RuL(cod)] complex, the angle (−33.8°) is forced by the coordination geometry imposed by the presence of the cyclic olefin. We can also see that [NiL] almost lies on the curve maximum. On account of the crystal-field stabilisation energy for a d^8 ion, Ni^{II} is indeed comfortable in a square-planar coordination environment. As the four nitrogen donor atoms in [NiL] lie in the same plane with the metal atom, the N2-C6-C7-N3 torsion angle can assume only small values. In contrast, there is no crystal-field stabilisation energy for the spherical, high-spin Mn^{II} ion. The ligand is then free to assume its preferred conformation around the metal atom in **4**.

The *o*-phenylene bridge, in contrast, forces the square-planar arrangement of the N_4 set around a single manganese ion. This tetradentate ligand arrangement is most commonly observed in Mn Schiff base complexes.[13, 14] The structure of **5** is shown in Figure 4. There are two molecules in the

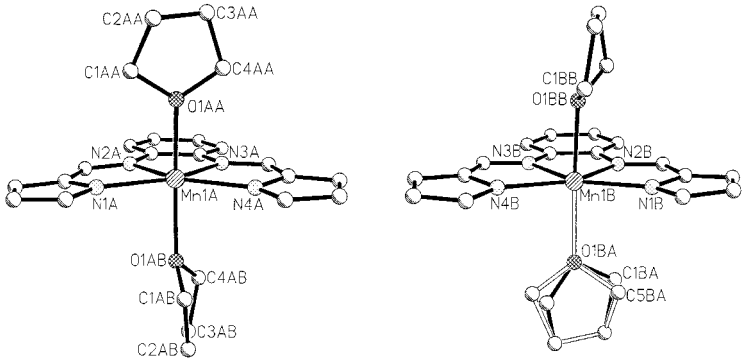

Figure 4. XP view of complex **5**. Left: molecule A, right: molecule B. Note that the only difference between the two molecules is the orientation of the THF ligands and that one of these is disordered in molecule B.

asymmetric unit. The two independent L′ ligands can be perfectly super-imposed and the metal coordination sphere is almost the same in the two cases. The only difference between the two molecules is in the orientation of the THF molecules (Table 1 and Figure 4). In complex B, one of the THF molecules is disordered and two conformations were refined, while complex A is completely ordered. The angle between the mean planes of the two THF conformations in the disordered THF is 27.8(6)°. The fact that two molecules are present in the asymmetric unit is probably the result of close-packing requirements.

Reactivity of Mn^{II} complexes with molecular dioxygen: Compounds **4**–**6** are particularly remarkable in the field of manganese chemistry for several reasons: i) they contain an N_4 ligand set which is quite unusual for manganese except for the porphyrin derivatives, ii) in complex **4** we have a preorganised dimetallic system in which the two metals are in close proximity within a protecting cavity and which exemplifies the ideal structural model for the two-electron (peroxo) or four-electron (oxo) reduction of dioxygen and

iii) in complexes **5** and **6**, pyrophen (L in **1**) can easily rearrange to a dinucleating ligand, like the analogous salophen (phenyl rings instead of pyrrole), so that under redox conditions **5** and **6** will behave in a similar manner to **4**.[13b, 15]

Although much chemistry deals with the manganese-oxo functionality, its synthesis is essentially confined to hydrolysis/oxidation of Mn^{II} and Mn^{III} complexes by peroxides[16] or other oxo-transfer agents (PhIO, etc.).

The reaction of Mn^{II} and Mn^{III} derivatives with dioxygen, although particularly relevant, has been poorly explored because of the possible formation of by-products derived from the oxidative degradation of the ligand in addition to the expected peroxo, superoxo and oxo species.[17, 18] At this stage, however, we should mention two important exceptions, namely the formation of two dinuclear Mn-peroxo species directly from molecular oxygen.[19, 20] These compounds may be the plausible precursors that precede the formation of di-μ-oxo-Mn^{IV} species.

The reactions of **4**–**6** with dioxygen (Schemes 3 and 4) were carried out under rigorous anhydrous conditions to avoid the complication derived from a parallel or subsequent hydrolysis

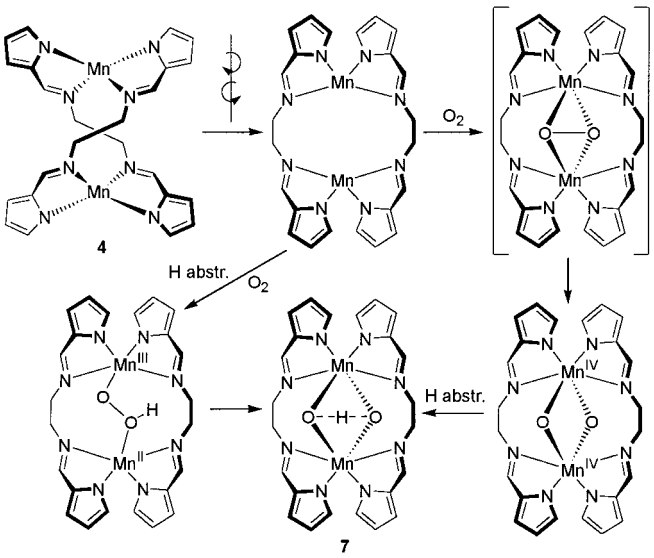

Scheme 3. The reaction of **4** with O_2 and the twisting rearrangement to give **7**.

reaction. In all cases, the gas-volumetric measurements showed the absorption of O_2 with a molar ratio O_2:Mn of 1:2. Complexes **7**–**9** were fully characterised, including the X-ray analyses of **7** and **9**. These last compounds have similar structures, despite the difference in the structure of the starting compounds **4** and **6**. It must be mentioned at this point that it is not uncommon to observe the salophen rearrangement to a dinucleating ligand under redox conditions.[13b, 15] Therefore, we can assume that at a certain stage [Mn(pyrophen)] (**6**) displays a dinuclear structure analogous to **4**, preceding the reaction with dioxygen. The dimer **4** already has a preorganised cavity to host a dioxygen molecule. This cavity is not easily accessible when the molecule is in its helical form; however, sufficient space to host O_2 becomes available after a

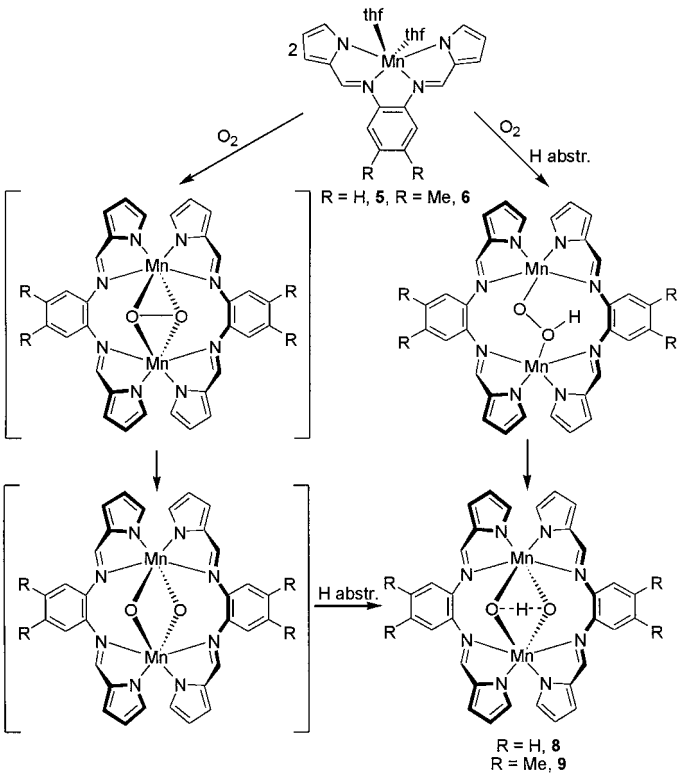

Scheme 4. The reaction of mononuclear complexes **5** and **6** with O_2 to give binuclear complexes **8** and **9**.

twisting rearrangement that sterically reorganises the ligands around the metal–metal axis, as shown in Scheme 3. Compound **7** was obtained as a black powder. On account of its remarkable insolubility, suitable crystals for X-ray analysis were grown directly in the reaction vessel by exposure of a diluted solution of **4** to dry oxygen (see the Experimental Section). The crystal structure of **7** is shown in Figure 5. Its determination was handicapped by the combination of a poorly diffracting sample, disorder, seen as diffuse scattering

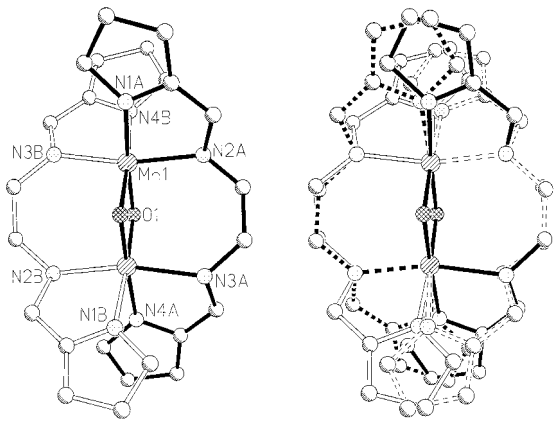

Figure 5. XP view of complex **7**. Left: view of the two ligands used to parameterise the disorder. Both manganese and oxygens atoms are shown. Note that the data do not permit a determination of whether this conformation is the correct one. Ligand A has solid bonds while ligand B has open bonds. Right: The complete average molecular structure illustrating the strong ligand disorder. The two A ligands have solid and dashed solid bonds while the two B ligands have open and dashed open bonds, respectively.

0947-6539/01/0707-1472 $ 17.50+.50/0 *Chem. Eur. J.* **2001**, *7*, No. 7

on the diffractograms, and the presence of non-merohedral twinning. The structure could, however, be modelled successfully as an ordered Mn–O core (with the same oxo/hydroxo disorder as in **9**) surrounded by disordered ligands. The ligand disorder was modelled by a superposition of ligands with the pyrrolyl groups *trans* to the Mn-Mn-N2-N3 plane. This is opposite to what was observed for **9** (see below). While this gave a good model, we cannot, with certainty, determine whether the *trans* geometry is the correct one. It is clear from the many attempts which we have performed that this structure could not have been determined without the high flux and beam quality of the synchrotron. This illustrates one of the many beneficial uses of synchrotron radiation in chemistry. It is worth noting that the data collection time for this crystal was less than four hours, which demonstrates that the combination of synchrotron radiation and area detectors can act as a fast, reliable tool.

Crystals of **9** suitable for X-ray analysis were grown in ethyl acetate. The complex (Figure 6) is situated on an inversion

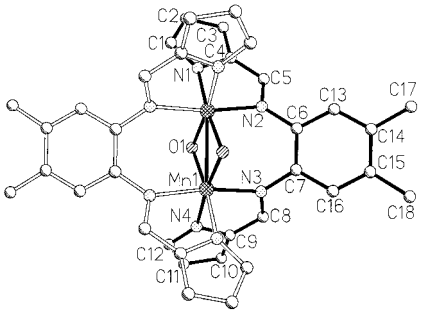

Figure 6. XP view of complex **9**.

centre in the crystal structure so that only half a molecule is present in the asymmetric unit. In addition, two solvent molecules are present per complex (one in the asymmetric unit). The carbonyl group of the ester is connected to the complex by two C–H···O hydrogen bonds C16–H16···O102B and C1–H1···O102A. They have the geometric characteristics C16···O102B = 3.519(11) Å and C16–H16···O102B = 173.8° and C1···O102C = 3.548(11) and C1–H1···O102C = 150.6° (B indicates the symmetry operation $x, y + 1, z + 1$ and C the symmetry operation $1 - x, -y - 1, -z - 1$). We observe a difference in the bond lengths of Mn1···O1 and Mn1···O1A (Table 1). On account of the crystal symmetry, the bonding situation is equivalent for the two manganese atoms. Therefore, the cause of the difference in the bond lengths is not clear: it could be the combination of oxo/hydroxo and oxidation-state disorder. In general, the Mn–O bond length in mixed-valent oxo/hydroxo bridged Mn^{III}/Mn^{IV} complexes is not a useful criterion to distinguish the oxidation state of the metal atoms.[21] This is especially true in the present case, in which the dinucleating ligands force the two manganese cations to remain at a distance that is shorter that 2.7 Å.

The genesis of **7**, **8** and **9** deserves a particular comment because of their relevance in the redox chemistry of Mn^{II}. Two possible pathways in Schemes 3 and 4 have been proposed. The first one reports the intermediate formation of a peroxo species that bridges the Mn^{III}/Mn^{III} centres, followed by the cleavage of the O–O bond to form a bis-μ-oxo dinuclear Mn^{IV} complex. It has been recently reported that such compounds promote hydride transfer[22] or hydrogen abstraction[23] in Mn-mediated hydrocarbon oxidations. This pathway seems rather unlikely because of the absence of such a reactivity in the analogous derivatives $[Mn_2(R\text{-salophen})_2(\mu\text{-}O)_2]$.[15] The alternative proposed pathway foresees the formation of an hydroperoxo Mn^{II}/Mn^{III} species as a result of the reaction of a single Mn^{II} with O_2 to give a mononuclear Mn^{III}-superoxo species capable of abstracting an hydrogen atom from the organic surroundings. The cleavage of the O–O bond leads directly to Mn^{III}/Mn^{IV} μ-oxo-μ-hydroxo species, **7**–**9**. Such a pathway has a significant support in the Mn-assisted intramolecular oxidation of the salophen ligand.[18]

Extended Hückel calculations[24] were performed on [Mn(pyrophen)] in order to investigate which frontier orbitals are available in the preliminary stage in the reaction with dioxygen. The molecular orbitals of the [Mn(pyrophen)] fragment are given on the left of Figure 7. The metal orbitals

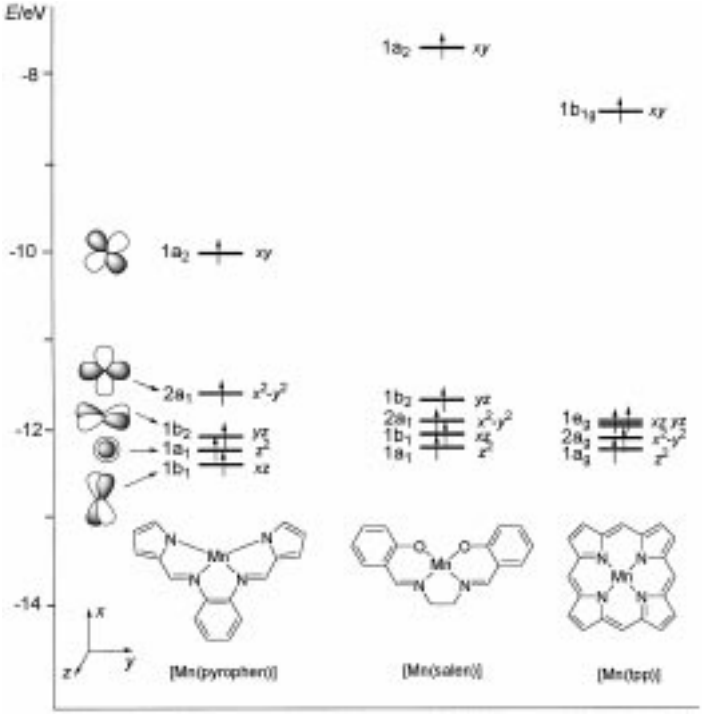

Figure 7. Molecular orbital diagram for [Mn(pyrophen)], [Mn(tpp)] and [Mn(salen)]. (For the sake of clarity the four phenyl rings attached to the main porhyrin skeleton of tpp have been omitted.)

mix strongly with the ligand frontier orbitals so that no pure d orbitals can be assigned. However, five MOs with large metal d character can be identified. These are the three closely spaced $1b_1(d_{xz})$, $1a_1(d_{z^2})$ and $1b_2(d_{yz})$ orbitals, which all lie within 0.2 eV, the $a_1(d_{x^2-y^2})$ orbital placed $\approx$0.5 eV above and the higher lying $a_2(d_{xy})$ orbital, which points more closely towards the nitrogen atoms of the ligands.

It is worth comparing the frontier orbitals of the [Mn(pyrophen)] fragment with those of [Mn(tpp)] and [Mn(salen)],

which have also been widely used in Mn-assisted catalytic oxygen-transfer reactions. The frontier orbitals of these two fragments are reported on the right of Figure 7. We note that [Mn(tpp)] and [Mn(salen)] have a similar ordering of the metal orbitals that is characterised by four closely spaced orbitals, d_{xz}, d_{yz}, d_{z^2} and $d_{x^2-y^2}$, which all lie within 0.3 – 0.4 eV, and a high-lying d_{xy} that points more directly towards the ligand atoms. The main differences between the frontier orbitals of these two fragments and those of [Mn(pyrophen)] lie in the higher energy of the $d_{x^2-y^2}$ and the lower energy of d_{xz} calculated for the [Mn(pyrophen)] fragment. Such a difference in the energy distribution of frontier orbitals may be important in the bonding mode of the O_2 in the preliminary stage of its interaction with the metal, as well as in the metal-assisted cleavage of the O – O bond leading to the formation of the oxo species.

Magnetic analysis of Mn^{II}-oxo and Mn^{III}/Mn^{IV}-oxo complexes: The magnetic susceptibilities of complexes **4** – **9** were measured in the temperature range 1.9 – 300 K and those of **4** and **7** – **9** are shown in Figures 8 and 9, respectively. The temperature dependence of the magnetic moment of **4** is typical of antiferromagnetic-coupled Mn^{II} dimers. The data were fitted with a theoretical equation [Eq. (1)],[25] based on the Heisenberg model $H = -2JS_1S_2$ ($S_1 = S_2 = 5/2$):

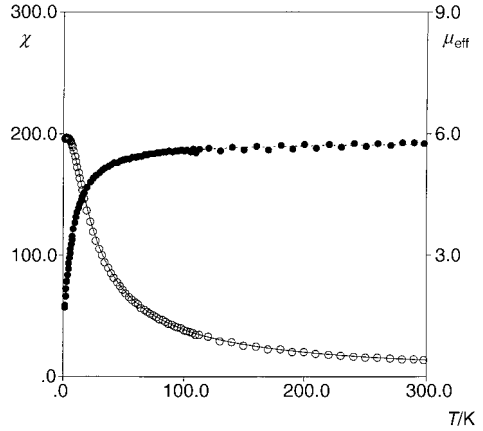

Figure 8. Magnetic susceptibilities (○) and effective magnetic moments (●) for complex **4**.

$$\chi_{dim} = \frac{Ng^2\mu_B^2}{kT}\,\frac{2e^{2x} + 10e^{6x} + 28e^{12x} + 60e^{20x} + 110e^{30x}}{1 + 3e^{2x} + 5e^{6x} + 7e^{12x} + 9e^{20x} + 11e^{30x}} \qquad (1)$$

where $x = J/kT$.

To obtain a good fit we included a correction for a small quantity of monomeric Mn^{II} impurities that were assumed to obey the Curie law. Equation (2) was therefore used for the total susceptibility:

$$\chi = 1/2(1-p)\chi_{dim} + p\frac{Ng'^2\mu_B^2 S(S+1)}{3kT} \qquad (2)$$

where $S = 5/2$, g' is the g factor of the impurity (assumed to be 2.00) and p is the monomeric impurity fraction. The value of g was fixed at 2.00, as expected for such a d^5 ion. The best fit to the collected data was obtained for $J = -1.0\ cm^{-1}$ and $p =$ 0.9 % (Figure 8). It is worth noting that the calculated coupling constant ($J = -1.0\ cm^{-1}$) is much smaller than that observed for the Cu^{II} $[Cu_2L_2]$ dimer ($J = -61.2\ cm^{-1}$),[8] which has the same connectivity as **4**. This is probably caused by the different magnetic orbitals involved in the two complexes as well as by the different coordination geometry of the two metal ions (quasi square-planar for the Cu^{II} centres, and almost tetrahedral for the Mn^{II} centers). The temperature dependence of the magnetic moment of **5** and **6** is typical of a high-spin Mn^{II} d^5 monomer ($S = 5/2$); the magnetic moment is nearly constant throughout the whole temperature range 2 – 300 K with a value of 5.85 and 5.90 μ_B, respectively.

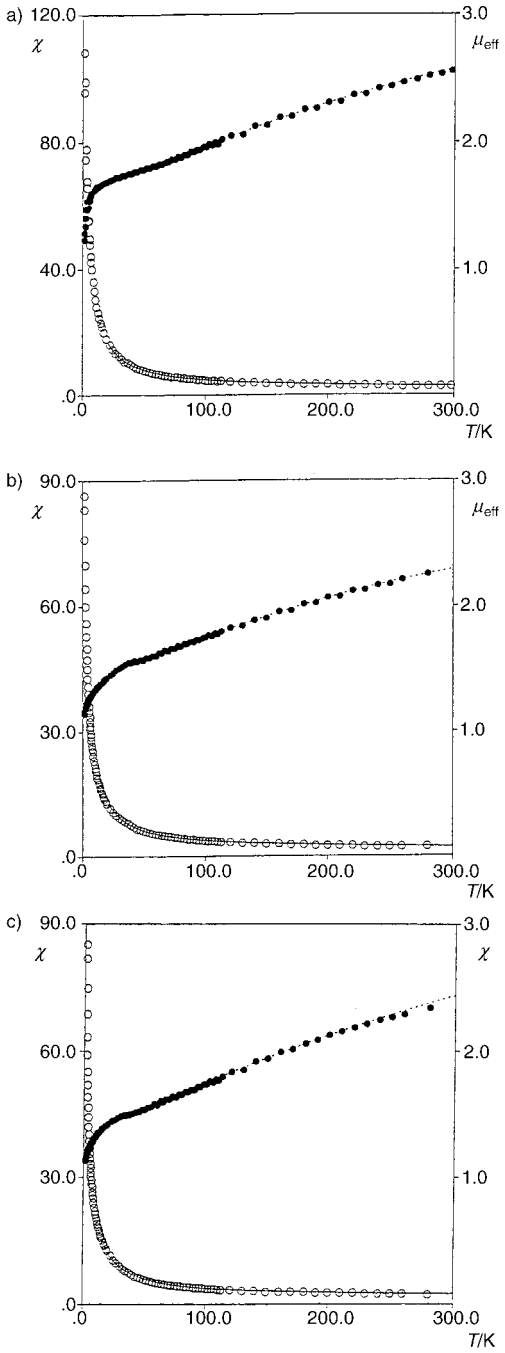

Figure 9. Magnetic susceptibilities (○) and effective magnetic moments (●) for complexes a) **7**, b) **8** and c) **9**.

0947-6539/01/0707-1474 $ 17.50+.50/0 *Chem. Eur. J.* **2001**, *7*, No. 7

For compounds **7**–**9**, the effective magnetic moments per manganese at room temperature are in the range 2.2–2.4 μ_B and decrease monotonically to approach a plateau of ≈1.4–1.6 μ_B below 60–80 K. A further irregular decrease is observed below 20–30 K; however, this can probably be attributed to the presence of paramagnetic impurities and/or small intermolecular interactions. The low-temperature values of the magnetic moments, 1.4–1.6 μ_B, correspond fairly well to the spin-only moment of 1.42 μ_B expected for an unpaired electron on the whole dimer, that is, for an $S = ½$ ground state; this suggests a strong antiferromagnetic coupling within the Mn^{III}/Mn^{IV} dimer.

The magnetic susceptibility data can be fitted by the spin-Hamiltonian given in Equation (3).

$$H = \mu_B H(g_1 S_1 + g_2 S_2) - 2JS_1S_2, \quad (3)$$

where $S_1 = 2$ is the spin of the Mn^{III} centre, $S_2 = ⅔$ is the spin of the Mn^{IV} centre and g_1 and g_2 are their g factors, which were assumed to be identical ($g_1 = g_2$). The susceptibility for such a system is calculated by means of the thermodynamic relationship $\chi = M/H$, where M is defined in Equation (4):

$$M = \frac{N\sum_i (-dE_i/dH)\, e(-E_i/k_B T)}{\sum_i e(-E_i/k_B T)} \quad (4)$$

The energy levels of the dimer, E_i, were evaluated by diagonalising the 20×20 Hamiltonian matrix in the basis that contained the product of the spin functions for the two single-spin centres. Because of the anomalous behaviour below 20–30 K, a best fit to the experimental data was performed only above 30 K and included a correction for the presence of monomeric Mn^{III} impurities, as described above.

The best-fit parameters are $g = 1.98$, $J = -53\ cm^{-1}$, $p = 4.4\%$ for **7**; $g = 1.92$, $J = -64\ cm^{-1}$, $p = 2.8\%$ for **8** and $g = 1.91$, $J = -60\ cm^{-1}$, $p = 3{,}9\%$ for **9**. These values of the Heisenberg coupling constant are somewhat smaller than those observed for mixed-valent bis(μ-oxo)dimanganese(III/IV) complexes,[1b, 1g] which fall in the range -100 to $-250\ cm^{-1}$, and are close to the values observed for mono(μ-oxo)-dimanganese(III/IV) complexes with other ligands less effective for magnetic superexchange, such as (μ-oxo)(μ-CH_3CO_2)-dimanganese(III/IV), with $J = -40\ cm^{-1}$.[26]

Experimental Section

General procedure: All reactions were carried out in an atmosphere of purified nitrogen. Solvents were dried and distilled before use by standard methods. $[Mn_3(Mes)_6]\cdot$toluene was prepared according to a published procedure.[27] NMR and ESR spectra were recorded on AC200 Bruker spectrometer. Infrared spectra were recorded with a Perkin–Elmer FT1600 spectrophotometer. Oxygen uptake was measured in THF at 288 K according to a modified version of an apparatus previously reported.[28]

Synthesis of LH_2 (1): Ethylenediamine (15 mL, 225 mmol) was slowly added at room temperature to a solution of pyrrole-2-carboxaldehyde (42.34 g, 450 mmol) in ethanol (300 mL). The mixture was heated under reflux overnight. A white solid precipitated that was collected and extracted with ethanol (300 mL). White crystals of LH_2 were collected and dried in vacuo (44.35 g, 92%). ^{1}H NMR (200 MHz, [D$_6$]DMSO, 25 °C): $\delta = 11.36$ (br s, 1H; NH), 8.06 (s, 1H; CH=N), 6.84 (t, $J = 4$ Hz, 1H), 6.41 (m, CH), 6.08 (t, $J = 4$ Hz, 1H), 3.72 (s, 2H; CH_2).

Synthesis of $L'H_2$ (2): 1,2-Phenylenediamine (11.4 g, 105 mmol) was added to a CH_2Cl_2 (200 mL) solution of pyrrol-2-carboxyaldehyde (20.0 g, 210 mmol). The resulting dark solution was stirred for 48 h, and then the solvent was evaporated at reduced pressure. The residue was suspended in hexane and stirred for 30 min. A yellow microcrystalline product was collected and dried in vacuo (22 g, 81%). ^{1}H NMR (200 MHz, CD_2Cl_2, 25 °C): $\delta = 12.27$ (br s, 1H; NH), 7.77 (s, 1H; CH=N), 7.28 (t, $J = 4$ Hz, 1H), 7.14 (m, 1H), 6.44 (t, $J = 4$ Hz, 1H), 6.26 (m, 1H), 6.03 (m, 1H).

Synthesis of $L''H_2$ (3): 4,5-Dimethyl-1,2-phenylenediamine (11.9 g, 87 mmol) was added to a solution of pyrrol-2-carboxyaldehyde (16.7 g, 175 mmol) in CH_2Cl_2 (150 mL). The resulting dark red solution was stirred for 15 min, then allowed to stand at 5 °C for 3 d. A yellow crystalline product was collected and dried in vacuo (18.4 g, 73%). ^{1}H NMR (200 MHz, [D$_6$]DMSO, 25 °C): $\delta = 11.53$ (br s, 1H; NH), 8.19 (s, 1H; CH=N), 6.95 (t, $J = 4$ Hz, 1H), 6.82 (m, 1H), 6.60 (t, $J = 4$ Hz, 1H), 6.16 (m, 1H), 2.21 (s, 3H; CH_3). Crystals suitable for X-ray analysis were grown in CCl_4 at room temperature.

Synthesis of 4: $[Mn_3(Mes)_6]\cdot$toluene (8.46 g, 8.7 mmol) was added to a solution of **1** (5.64 g, 26.2 mmol) in toluene (400 mL) to give a yellow suspension that was heated under reflux for 4 h. A red microcrystalline solid was collected and dried in vacuo (6.38 g, 91%). IR (Nujol): $\tilde{\nu}_{max}$ = 1594 (s), 1438 (s), 1395 (m), 1342 (m), 1330 (w), 1305 (s), 1191 (w), 1035 (s), 980 (m), 797 (w), 745 (s), 735 (s), 609 (w), 595 (w), 445 cm^{-1} (w); elemental analysis calcd (%) for $C_{12}H_{12}MnN_4$ (267.2): C 53.94, H 4.53, N 20.97; found C 53.94, H 4.46, N 20.62. Crystals suitable for X-ray analysis were grown slowly by cooling a hot toluene solution to room temperature.

Synthesis of 5: $[Mn_3(Mes)_6]\cdot$toluene (3.74 g, 3.85 mmol) was added to a solution of **2** (3.03 g, 11.6 mmol) in THF (200 mL) to give a brown suspension that was heated under reflux for 4 h. This suspension was concentrated to 50 mL and then *n*-hexane (100 mL) was added. The yellow-brown solid was collected and dried in vacuo (4.90 g, 92%). IR (Nujol): $\tilde{\nu}_{max}$ = 1592 (s), 1560 (s), 1440 (m), 1385 (s), 1300 (s), 1189 (w), 1030 (s), 973 (m), 875 (w), 820 (w), 757 (m), 745 (s), 616 (w), 592 (w), 575 (m), 485 cm^{-1} (w); elemental analysis calcd (%) for $C_{24}H_{28}MnN_4O_2$ (459.4): C 62.74, H 6.14, N 12.19; found: C 62.52, H 6.31, N 12.05. Crystals suitable for X-ray analysis were grown in THF/*n*-hexane at room temperature.

Synthesis of 6: $[Mn_3(Mes)_6]\cdot$toluene (3.31 g, 3 mmol) was added to a THF (120 mL) solution of **3** (2.16 g, 7.44 mmol) to give a brown suspension that was heated under reflux for 4 h. This suspension was concentrated to 50 mL and then *n*-hexane (90 mL) was added. The orange microcrystalline solid was collected and dried in vacuo (2.90 g, 80%). IR (Nujol): $\tilde{\nu}_{max}$ = 1595 (s), 1560 (s), 1440 (m), 1385 (s), 1300 (s), 1189 (w), 1030 (s), 973 (m), 875 (w), 820 (w), 757 (m), 745 (s), 616 (w), 592 (w), 575 (m), 485 cm^{-1} (w); elemental analysis calcd (%) for $C_{26}H_{32}MnN_4O_2$ (487.5): C 64.06, H 6.62, N 11.49; found: C 63.95, H 6.72, N 11.88.

Synthesis of 7: A yellow THF (200 mL) solution of **4** (1.11 g, 2.08 mmol) was exposed to dry O_2 to give a black suspension that was stirred overnight. The solid was collected and dried in vacuo (1.13 g, 96%). Gas-volumetric measurements showed that the solution had absorbed 0.94 mol of O_2 per mole of **4**. IR (Nujol): $\tilde{\nu}_{max}$ = 1576 (s), 1434 (s), 1389 (s), 1338 (m), 1267 (s), 1185 (m), 1030 (s), 893 (w), 730 (s), 628 cm^{-1} (s); elemental analysis calcd (%) for $C_{24}H_{25}Mn_2N_8O_2$ (567.4): C 50.80, H 4.44, N 19.75; found: C 50.99, H 4.53, N 19.51. Crystals suitable for X-ray analysis were grown by allowing O_2 to diffuse slowly into a solution of **4** in THF (1.2×10^{-4} M) at room temperature.

Synthesis of 8: An orange solution of **5** (1.03 g, 2.24 mmol) in THF (200 mL) was exposed to dry O_2 to give a dark green suspension that was stirred overnight. The solid was collected and dried in vacuo (0.56 g, 76%). Gas-volumetric measurements showed that the solution had absorbed 0.54 mol of O_2 per mole of **5**. IR (Nujol): $\tilde{\nu}_{max}$ = 1552 (s), 1463 (s), 1381 (s), 1295 (s), 1267 (m), 1192 (w), 1040 (s), 988 (w), 889 (w), 752 (m), 741 (s), 648 (m), 423 cm^{-1} (w); elemental analysis calcd (%) for $C_{32}H_{25}Mn_2N_8O_2$ (663.5): C 57.93, H 3.80, N 16.89; found: C 57.77, H 3.58, N 16.59.

Synthesis of 9: An orange solution of **6** (4.53 g, 9.29 mmol) in THF (220 mL) was exposed to dry O_2 to give a dark green suspension that was stirred overnight. The solid was collected and dried in vacuo (2.41 g, 72%). Gas-volumetric measurements showed that the solution had absorbed 0.54 mol of O_2 per mole of **6**. IR (Nujol): $\tilde{\nu}_{max}$ = 1550 (s), 1463 (s), 1385 (s),

1298 (s), 1267 (m), 1192 (w), 1040 (s), 988 (w), 889 (w), 752 (m), 741 (s), 648 (m), 423 cm^{-1} (w); elemental analysis calcd (%) for $C_{36}H_{33}Mn_2N_8O_2$ (719.6): C 60.09, H 4.62, N 15.57; found: C 60.41, H 4.75, N 15.48.

Magnetic susceptibility measurements: Magnetic susceptibility was measured on a Quantum Design MPMS5 SQUID susceptometer operating at a magnetic field strength of 1 kOe. Corrections were applied for diamagnetism calculated from Pascal constants.[29] Effective magnetic moments were calculated as $\mu_{eff} = 2.828(\chi_{Mn}T)^{1/2}$, where χ_{Mn} is the magnetic susceptibility per manganese atom. Fitting of the magnetic data to the theoretical expression was performed by minimising the agreement factor defined in Equation (5) through a Levenberg–Marquardt routine.

$$\Sigma\frac{[\chi_i^{obsd}T_i - \chi_i^{calcd}T_i]^2}{(\chi_i^{obsd}T_i)^2} \quad (5)$$

PM3 calculations: PM3 calculations were performed with Gaussian 98.[12] LH_2 and $L'H_2$ were constructed from the experimental structures (from **4** for LH_2 and **5** for $L'H_2$) by adding hydrogens onto nitrogens N1 and N4. The structures were first optimised and then relaxed potential-energy scans of the N2-C6-C7-N3 torsion angle were carried out (one optimisation per degree).

Extended Hückel calculations: Extended Hückel calculations were performed with the CACAO molecular orbital program,[30] and parameters that have already been published.[31]

X-ray crystallography for complexes 3, 4, 5, 7 and 9: Suitable crystals were mounted in glass capillaries and sealed under a nitrogen atmosphere. All structures were solved and refined in SHELX.[32, 33] Crystal data are reported in Table 2. With the exception of **7** (vide infra), the structure solution was straightforward. Direct methods were used for all structures, as implemented in SHELXS-97.[32]. All structures were refined with full-matrix least-squares on F^2. When not stated otherwise, all non-hydrogen atoms were refined with anisotropic displacement parameters. Hydrogens were included in the "riding" model with $U_{iso} = aU_{eq}(X)$, where $a = 1.5$ for methyl and 1.2 for others and X is the parent atom. The anisotropic weighting scheme of SHELXL:[33] $w = 1/(\sigma^2(F_o^2) + (aP)^2 + bP)$, where $P = (\max(F_o^2,0) + 2F_c^2)/3$ was used throughout. In neither of the oxidised complexes (**7** and **9**) were we able to locate the oxygen-bound hydrogen. It is disordered in both structures. The program XP[34] was used for the graphical representation of all compounds.

Complex ***3***: Low-temperature diffraction data were collected on a MAR 345 imaging-plate detector system operating with 150 μm pixel size, 345 mm diameter active area and $Mo_{K\alpha}$ radiation. Data reduction was performed with DENZO and SCALEPACK.[35] From the visual inspection of the images, it was evident that two crystals contribute to the diffractograms. One of these dominated and so the data reduction was performed considering only this crystal (it was also evident that this was not caused by twinning). This means that the intensities of some low-order reflections might have been contaminated by the other crystallites. The 10534 measured reflections averaged to 5730 unique ones, $R_{int} = 0.034$. The lowest order reflections (to $d = 1.94$ Å) merged less than the next shell ($d = 1.94 - 1.54$ Å). This, together with an apparent error in the intensities of the low-order reflections seen during the refinement, led us to use only the 5209 unique reflections in the range $d = 1.89 - 0.85$ Å. The structure solution revealed that, in addition to the presence of two molecules of **3**, the asymmetric unit also contains a strongly disordered CCl_4 solvent molecule. The disorder was modelled by splitting the chlorine atoms into several contributing atoms. The C–Cl bond length was restrained to a common value, d_{C-Cl}, which was refined as a free variable. The restraints were given a standard uncertainty of 0.01 Å. In addition, the sum of the occupancies for each chlorine was restrained to 1.000(1). All contributing chlorines were refined with anisotropic displacement parameters that were restrained to be isotropic (s.u. 0.1). The total number of restraints was 88. The refined value of d_{C-Cl} was 1.746(4) Å. Hydrogens on the methyl groups were included as a rotating riding group (i.e. one torsion angle was optimised for the three hydrogens together, bond lengths and angles being fixed).

Complex ***4***: Data were collected at 293 K on a KUMA four-circle diffractometer equipped with a scintillation detector.

Complex ***5***: Data were collected on a Rigaku AFC6S four-circle diffractometer at 138 K and reduced with teXsan.[36] There are two molecules in the asymmetric unit and in one of these molecules one of the THF molecules is disordered. This disorder was modelled by allowing two conformations for C1 and C4 each with equal occupation. The two disordered atoms were refined with isotropic displacement parameters, while the other three were refined anisotropically. The ratios of the largest and smallest eigenvalue of the anisotropic displacement parameter tensor of the three non-split atoms are large which indicates that some disorder remains. This could not, however, be modelled in more detail.

Complex ***7***: Several crystals were examined in the laboratory. They all diffracted very poorly and none yielded structure solutions. Therefore, we collected data at the Swiss–Norwegian Beam Line (SNBL) at the European Synchrotron Radiation Facility (France). The SNBL is situated at a bending magnet. The optics of the beam line consist of an Rh-coated vertically collimating mirror followed by a sagitally focusing Si(111) double-crystal monochromator (focusing in the horizontal plane) and a Rh-

Table 2. Crystal data and structure refinements for **3**, **4**, **5**, **7** and **9**.

	3	**4**	**5**	**7**	**9**
formula	$2(C_{18}H_{18}N_4)\cdot CCl_4$	$C_{12}H_{12}MnN_4$	$C_{24}H_{28}N_4O_2Mn$	$C_{24}H_{25}N_8O_2Mn$	$C_{36}H_{33}N_8O_2Mn\cdot 2(C_4H_8O_2)$
M_w	734.54	534.39	459.44	567.40	895.79
T [K]	143(2)	293(2)	138(2)	293(2)	133(2)
λ [Å]	0.71073	0.71073	1.54184	0.8002(1)	0.71073
crystal system	triclinic	monoclinic	monoclinic	monoclinic	triclinic
space group	$P\bar{1}$	$C2/c$	$P2_1/n$	$P2_1/n$	$P\bar{1}$
a [Å]	10.411(2)	16.676(5)	16.42(3)	15.175(3)	8.5849(17)
b [Å]	13.359(3)	11.913(13)	13.22(2)	8.253(2)	10.787(2)
c [Å]	14.083(3)	12.569(18)	21.04(3)	12.295(3)	13.276(3)
α [°]	98.44(3)	90	90	90	103.43(3)
β [°]	91.58(3)	109.88(7)	104.38(13)	127.97(3)	102.38(3)
γ [°]	104.15(3)	90	90	90	105.74(3)
V [Å^3]	1874.5(7)	2348(4)	4422(14)	1228.6(4)	1099.2(4)
Z	2	4	8	2	1
ρ_{calcd} [g cm^{-3}]	1.301	1.512	1.380	1.534	1.353
μ [mm^{-1}]	0.354	1.105	5.079	1.067	0.630
absorption correction	none	none	ψ scans	none	none
reflections collected	10534	2123	4843	16479 (in super cell)	5396
data/parameters	5209/531	2123/154	4637/557	2069/132	2632/275
R_1 [$I > 2\sigma(I)$]	0.0512	0.0791	0.0641	0.0551	0.0874
wR_2 (all data)	0.1303	0.2386	0.1937	0.1481	0.2192

0947-6539/01/0707-1476 $ 17.50+.50/0 *Chem. Eur. J.* **2001**, *7*, No. 7

coated vertically focusing second mirror. The wavelength was set to 0.8002(1) Å. For the experiment we used a MAR345 imaging-plate detector operated with an effective diameter of 240 mm and 150 μm pixel size. The crystal used for measurements (several crystals were tested) was of poor quality, but sufficient for a data collection if an increased synchrotron flux was used. Data were collected with the oscillation method and a total of 158 frames of 2° oscillation each were collected. The peaks were all very large and anisotropic in shape; the oscillation angle was slightly dependent on the size. Many reflections resided on lines of weak, diffuse scattering which showed that the structure is disordered. The diffraction pattern was successfully indexed with DENZO[35] to a monoclinic cell of dimensions $a = 12.51$, $b = 8.25$, $c = 24.59$ Å and $\beta = 104.57°$. Integration was performed with DENZO[35] and the data were scaled to correct for the decay of the incident beam with SCALEPACK[35] in point group 2/*m*. Initial analysis of the diffraction pattern showed a set of non-space-group absences: all reflections with *h* even and *l* odd were absent. This led us to believe that the sample was a non-merohedral twin. A schematic view of the diffraction pattern in the a^*/c^* plane is shown in Figure 10a. The pattern can be explained if one assumes the presence of

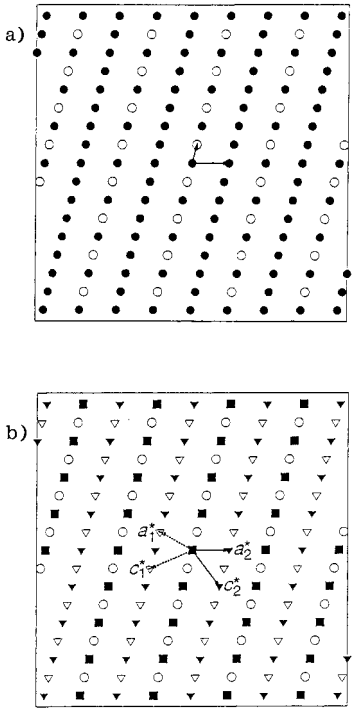

Figure 10. a) Schematic view of the observed diffraction pattern in the a^*/c^* plane of **7**. ○ represent systematically extinct reflections, while ● represent present reflections. The lattice vectors used for integration of the data are indicated. b) Decomposition of the observed pattern into reflections stemming from the two contributing domains. ○ represent the systematically absent reflections, ■ represent the common reflections, △ are pure domain 1 reflections and ▲ represent pure domain 2 reflections.

two domains linked by a two-fold rotation around the *b* axis (Figure 10b) The Miller indices (and, therefore, also the direct-space lattice vectors) are transformed according to $h_1 = (l-h)/2$, $k_1 = k$, $l_1 = -(h+l)/2$ and $h_2 = h + l/2$, $k_2 = -k$, $l_2 = -l/2$. The unit cell of each domain is also monoclinic with dimensions $a_2 = 15.175$, $b_2 = 8.253$, $c_2 = 12.295$ Å and $\beta_2 = 127.97°$. For the twinning to be exact (i.e. that the reflections common to the two domains overlap exactly), the metric must fulfill the condition $a = -2c\cos\beta$. If we write $c = 2a(1+\delta)$ this condition becomes $\cos\beta = -1/[4(1+\delta)]$. Here we have $\delta = -0.0172$ which leads to an expected value of $\beta = 104.74°$. This deviation of 0.17° is close to the resolution of the present experiment, which results from the poor crystal quality, hence no resolvable peak splitting could be observed. It was apparent that one domain dominated the diffraction pattern. If the relative average intensity of the 777 unique reflections in domain 1 are set to one, the relative average intensity of the 767 unique common reflections is 33.1, while that of the 778 unique reflections in domain 2 is 25.5. Thus, domain 1 accounts for only ≈4% of the superstructure scattering. The structure was therefore solved with direct methods and a data set that consists of the common reflections and the pure domain 2 reflections. In addition to the twinning, the structure also displays strong disorder. This is confirmed by the observation of diffuse scattering in the diffractograms. The symmetry of each domain is $P2_1/n$ with two formula units in the unit cell. This indicates that each complex is situated at a crystallographic point of symmetry higher than the molecular one. The manganese and oxygen are ordered, while the ligand is strongly disordered. We modeled the ligand disorder by placing two complete unique ligands on either side of the manganese atom, each with half occupancy. An open question is whether the conformation of the ligand was such that the pyrrolyl groups are on the same side of the N1-Mn-Mn-N4 plane as in **9** or on opposite sides. While we cannot decide this with certitude from the present data, the initial refinements made it clear that a model with unique ligands which both have the same conformation as **9** (one ligand having both pyrrolyl groups above and the other both below) does not fit the data for **7**. In our final model, the unique ligands have the pyrroles on either side of Mn-N plane (see Figure 5, left). This gives the disordered model shown in Figure 5 (right). Once this ligand description was employed, the refinement was remarkably well-behaved. At the final stages of the non-twinned refinement even hydrogens were visible in the difference map. The final cycles of the refinement included all data and the HKLF5 option of SHELXL[33] was used to describe the non-merohedral twinning. The model consisted of anisotropic manganese and oxygen. The ligands were described with isotropic displacement parameters that were constrained to be equal for equivalent atoms in the two ligands. All hydrogens, except for those on the oxygen, were included in the riding model as for the other structures. The final twinning volume ratio gave 97.10(5)% of domain 2 in good agreement with the estimate given above from the ratio of average intensities.

*Complex **9***: Data were collected at 133 K on a KUMA CCD and reduced with CrysAlis-RED.[37] The structure determination revealed that the complex is situated on an inversion centre. In addition to the complex, one ethyl acetate (solvent) is present in the asymmetric unit.

Crystallographic data (excluding structure factors) for the structures reported in this paper have been deposited with the Cambridge Crystallographic Data Centre as supplementary publication Nos. CCDC-147150 (**3**), CCDC-147151 (**4**), CCDC-147152 (**5**), CCDC-147153 (**7**) and CCDC-147154 (**9**). Copies of the data can be obtained free of charge on application to CCDC, 12 Union Road, Cambridge CB21EZ, UK (fax: (+44) 1223-336-033; e-mail: deposit@ccdc.cam.ac.uk).

Acknowledgements

We thank the "Fonds National Suisse de la Recherche Scientifique" (Bern, Switzerland, Grant No. 20-53336.98) for financial support and for access to the Swiss–Norwegian beam lines at ESFR in Grenoble (France). H.B. thanks the Danish Research Academy for financial support. The staff at the Swiss–Norwegian beam lines is acknowledged for their kind support.

[1] a) *Photosynthesis* (Ed.: W. R. Briggs); ARL, New York, **1989**; b) K. Wieghardt, *Angew. Chem.* **1989**, *101*, 1179–1198; *Angew. Chem. Int. Ed. Engl.* **1989**, *28*, 1153–1172; c) G. W. Brudwig, R. H. Crabtree, *Progr. Inorg. Chem.* **1989**, *37*, 99–142; d) *Manganese Redox Enzimes* (Ed.: V. L. Pecoraro), VCH, New York, **1992**; e) *The Photosynthetic Reaction Center, Vols. I and II* (Eds.: J. Deisenhofer, J. R. Norris), Academic, New York, **1993**; f) E. Gallo, E. Solari, S. De Angelis, C. Floriani, N. Re, A. Chiesi-Villa, C. Rizzoli, *J. Am. Chem. Soc.* **1993**, *115*, 9850–9851; g) R. Manchanda, G. W. Brudvig, R. H. Crabtree, *Coord. Chem. Rev.* **1995**, *144*, 1–38; h) G. C. Dismukes, *Chem. Rev.* **1996**, *96*, 2909–2906; i) J. Limburg, J. S. Vrettos, L. M. Liable-Sands, A. L. Rheingold, R. H. Crabtree, G. Brudvig, *Science* **1999**, *283*, 1524–1527; l) C. E. Dubé, R. Sessoli, M. P. Hendrich, D. Gatteschi, W. H. Armstrong, *J. Am. Chem. Soc.* **1999**, *121*, 3537–3538.

[2] S. I. Murahashi, T. Naota in *Comprehensive Organometallic Chemistry II: A Review of the Literature 1982–1994, Vol. 12* (Eds.: E. W. Abel,

F. G. A. Stone, G. Wilkinson), Pergamon, Oxford (UK), **1995**, Chapter 11.3.
[3] E. N. Jacobsen in *Comprehensive Organometallic Chemistry II: A Review of the Literature 1982–1994, Vol. 12* (Eds.: E. W. Abel, F. G. A. Stone, G. Wilkinson), Pergamon, Oxford (UK), **1995**, Chapter 11.1.
[4] M. Calligaris, L. Randaccio in *Comprehensive Coordination Chemistry, Vol. 2* (Eds.: G. Wilkinson, R. D. Gillard, J. A. McLeverty), Pergamon, Oxford (UK), **1987**, Chapt. 20.1.
[5] Hydrogen-bond geometries: D ··· A and D-A ··· A are 2.960(2) Å and 157.2° for N1A-H1A ··· N3B, 2.955(2) Å and 155.5° for N1B-H1B ··· N3A, 2.889(2) Å and 156.2° for N4A-H4A ··· N2B, 2.912(2) Å and 154.7° for N4B-H4B ··· N2A.
[6] C. Piguet, G. Bernardinelli, G. Hopfgartner, *Chem. Rev.* **1997**, *97*, 2005–2062.
[7] F. H. Allen, J. E. Davies, J. J. Galloy, O. Johnson, O. Kennard, C. F. Macrae, E. M. Mitchell, G. F. Mitchell, J. M. Smith, D. G. Watson, *J. Chem. Inf. Comput. Sci.* **1991**, *31*, 187–204.
[8] T. Kikuchi, C. Kabuto, H. Yokoi, M. Iwaizumi, W. Mori, *J. Chem. Soc. Chem. Commun.* **1983**, 1306–1307.
[9] F. Franceschi, C. Floriani, unpublished results.
[10] C. Stern, F. Franceschi, E. Solari, C. Floriani, N. Re, R. Scopelliti, *J. Organomet. Chem.* **2000**, *593*, 86–95.
[11] G. C. van Stein, G. van Koten, H. Passenier, O. Steinbach, K. Vrieze, *Inorg. Chim. Acta* **1984**, *89*, 79–87.
[12] *Gaussian 98* (Revision A.7), Gaussian, Inc., Pittsburgh, PA, **1998**.
[13] a) P. J. Pospisil, D. H. Carsten, E. N. Jacobsen, *Chem. Eur. J.* **1996**, *2*, 974–980; b) E. Gallo, E. Solari, N. Re, C. Floriani, A. Chiesi-Villa, C. Rizzoli, *J. Am. Chem. Soc.* **1997**, *119*, 5144–5154; c) L. Canali, D. C. Sherrington, *Chem. Soc. Rev.* **1999**, *28*, 85–93, and references therein.
[14] E. Gallo, E. Solari, C. Floriani, A. Chiesi-Villa, C. Rizzoli, *Inorg. Chem.* **1997**, *36*, 2178–2186.
[15] a) M. R. Bermejo, A. Castiñeiras, J. C. Garcia-Monteagudo, M. Ray, A. Sousa, M. Watkinson, C. A. McAuliffe, R. G. Pritchard, R. Beddoes, *J. Chem. Soc. Dalton Trans.* **1996**, 2935–2944; b) H. Torayama, T. Nishide, H. Asada, M. Fujiwara, T. Matsushita, *Polyhedron* **1998**, *17*, 105–118.
[16] V. L. Pecoraro in *Manganese Redox Enzymes* (Ed.: V. L. Pecoraro), VCH, New York, **1992**, Chapter 10, and references therein.
[17] V. L. Pecoraro, M. J. Baldwin, A. Gelasco, *Chem. Rev.* **1994**, *94*, 807–826, and references therein.
[18] E. Gallo, E. Solari, N. Re, C. Floriani, A. Chiesi-Villa, C. Rizzoli, *Angew. Chem.* **1996**, *108*, 2113–2115; *Angew. Chem. Int. Ed. Engl.* **1996**, *35*, 1981–1983.
[19] R. Bhula, G. J. Gainsford, D. C. Weatherburn, *J. Am. Chem. Soc.* **1988**, *110*, 7550–7552.
[20] U. Bossek, T. Weyhermüller, K. Wieghardt, B. Nuber, J. Weiss, *J. Am. Chem. Soc.* **1990**, *112*, 6387–6388.
[21] D. Ramalakshmi, M. V. Rajasekharan, *Acta Crystallogr. Sect. B* **1999**, *55*, 186–191, and references therein.
[22] M. Lockwood, K. Wang, J. M. Mayer, *J. Am. Chem. Soc.* **1999**, *121*, 11894–11895, and references therein.
[23] K. Wang, J. M. Mayer, *J. Am. Chem. Soc.* **1997**, *119*, 1470–1471.
[24] a) R. Hoffmann, W. N. Lipscomb, *J. Chem. Phys.* **1962**, *36*, 2179–2189; b) R. Hoffmann, *J. Chem. Phys.* **1963**, *39*, 1397–1412.
[25] O. Kahn, *Molecular Magnetism*, VCH, New York, **1992**.
[26] K. Wieghardt, U. Bossek, J. Bonvoisin, P. Beaullivain, J. J. Girerd, B. Nuber, J. Weiss, J. Heinze, *Angew. Chem.* **1986**, *98*, 1026–1027; *Angew. Chem. Int. Ed. Engl.* **1986**, *25*, 1030–1031.
[27] E. Solari, F. Musso, E. Gallo, C. Floriani, N. Re, A. Chiesi-Villa, C. Rizzoli, *Organometallics* **1995**, *14*, 2265–2276.
[28] F. A. Cotton, F. Calderazzo, *Inorg. Chem.* **1962**, *1*, 30–36.
[29] E. A. Boudreaux, L. N. Mulay, *Theory and Applications of Molecular Paramagnetism*, Wiley, New York, **1976**, pp. 491–495.
[30] C. Mealli, D. M. Proserpio, *J. Chem. Educ.* **1990**, *67*, 399–402.
[31] S. Alvarez, *Tables of Parameters for Extended Hückel Calculations*, Universitat de Barcelona, Barcelona (Spain), **1993**.
[32] G. M. Sheldrick, *SHELXS-97, Program for the Solution of Crystal Structures*, University of Göttingen, (Germany), **1997**.
[33] G. M. Sheldrick, *SHELXL-97, Program for the Refinement of Crystal Structures*, University of Göttingen, (Germany), **1997**.
[34] *XP 5.0.4*, Siemens Analytical X-ray Insts., **1996**.
[35] Z. Otwinowski, W. Minor, *Methods Enzymol. A* **1997**, *276*, 307–326.
[36] *teXsan 1.0.1 for Windows*, Molecular Structure Corporation, a Rigaku company, 3200 Research Forest Drive, The Woodlands, TX 77381–4238 (USA), **1997**.
[37] *CrysAlis-RED*, release 1.6.2, Kuma Diffraction Instruments GmbH, PSE-EPFL module 3.4, CH-1015, Lausanne (Switzerland), **1999**.

Received: July 19, 2000 [F2611]

  0947-6539/01/0707-1478 $ 17.50+.50/0